Optical Cross Connect Switch Based on Tip/Tilt Micromirrors in a White Cell

Betty Lise Anderson, *Senior Member, IEEE,* Victor Argueta-Diaz, Feras Abou-Galala, *Student Member, IEEE,* Gayathri Radhakrishnan, and Richard Joseph Higgins, *Member, IEEE*

***Abstract*—We present a new approach to optical interconnections, based on microelectromechanical system tip/tilt mirror technology and the White cell. This is a free-space approach in which many beams circulate simultaneously in the device, each beam forming a unique spot pattern on the micromirror array. On each bounce, each beam can be switched to any of several White cells, each of which has a different effect on the spot pattern. By appropriate combinations of these White cells, any input beam can be directed to any output. A simple proof-of-concept prototype has been demonstrated, and output coupling loss addressed.**

***Index Terms*—Microelectromechanical systems (MEMS) devices, optical communications, optical interconnections, White cell.**

I. Introduction

FINDING a way to perform routing and interconnection functions while keeping signals in the optical domain is still the number one problem to be solved in optical communications. This routing involves two separate functions: reading and interpreting the destination information in optical form, and switching the optical beams without converting to electronics. This paper concerns itself with the second of these.

Many approaches to the cross connect problem are found in the literature. At first, waveguide approaches involving arrays of waveguide switches appeared. Electrooptic [1], [2] or thermooptic switches [3] typically cascade 2×2 switches for larger numbers of inputs and outputs. For example, a 16×16 thermooptic switch requires 256 individual switches [4]. The waveguide solution is not expected to scale up much more than perhaps a hundred inputs and outputs because the planar two-dimensional (2-D) approach necessarily requires all of the input and outputs to be in a single plane, and the integrated optics circuit substrates can only be so large. There is also the issue of coupling losses in going from circular fibers into rectangular waveguides and back.

Next are the interconnects based on microelectromechanical systems (MEMS) devices, of which many ingenious types have been proposed and implemented. These may be classified as 2-D and three-dimensional (3-D). In 2-D interconnections, the inputs and outputs all lie in a single plane, the plane containing the MEMS mirror switches. One example of a 2×2 crossbar switch has four fibers that are arranged in an "X," and a tiny mirror slides in and out of the intersection [5]. Thus, light beams either cross unimpeded to the fiber opposite them or get diverted into fiber next door. Another device uses a linear array of input fibers along one edge of the chip and another array along an adjacent edge. Micromirrors pop up and down to divert each beam to its intended destination [6]. This is an example of an N^2 interconnection, where N is the number of inputs and outputs, and N^2 represents the total number of pixels required.

Three-dimensional approaches are those in which the inputs and outputs are arranged facing the MEMS mirror rather than along its edges. Usually, the input–output fibers are in a 2-D array, and light from these strikes the MEMS mirror from above. The beams are reflected such that they are output to a different fiber array, or else to the same array but at different fibers. Until recently, the classic example of this approach was being marketed by Lucent [7] who reported a 1024×1024 cross connect. This is an example of a $2N$ solution, requiring $2N$ pixels for N ports. The 3-D approach is ultimately the most scalable and, thus, the most practical long-term solution.

Solutions that are 3-D involve free space, with the beams diverging as they propagate from one element to another. Although the beams can be collimated to some extent, these approaches will be limited in how far a beam can be transmitted before becoming too large. A significant distance may be required, however, for a beam to go, say, from the first input to the last output.

We take a new approach to the optical cross connect problem. We also use a 3-D, free-space approach, using MEMS mirrors as switches. Our concept, however, is based on the White cell, a system of three spherical mirrors between which light circulates an arbitrary number of times. In the White cell, beams are refocused to spots on each pass. We will arrange these spots to land on the individual pixels of a MEMS mirror, and thus, have the opportunity to switch a beam toward a new destination on each pass. We will show that the spots form in rows and columns, and by switching between various White cells with the MEMS mirrors, we can shift each beam's spot pattern by a controlled number of rows such that it comes out at a predetermined output location.

First, in Section II, we will review the White cell, paying special attention to the spot patterns generated in them. In Section III, we will present a simple optical interconnection device and discuss its operation. In Section IV, we will point out the need for beam combiners at the outputs and present two solutions. In Section V, we extend our designs to allow many more inputs and outputs for the same number of bounces, a necessary improvement

Manuscript received September 24, 2002; revised March 3, 2003. This work was supported in part by OptiConnect, Columbus, OH USA.

B. L. Anderson, V. Argueta-Diaz, F. Abou-Galala, and G. Radhakrishnan are with The Ohio State University, Columbus, OH 43210 USA (e-mail: Anderson@ee.eng.ohio-state.edu; Argueta-Diaz.1@osu.edu; abou-galala.1@osu.edu; radhakrishnan.2@osu.edu).

R. J. Higgins is with Optimer Photonics, Columbus, OH 43201 USA (e-mail: higginsr@battelle.org).

Digital Object Identifier 10.1109/JSTQE.2003.813303

as the demand for larger and larger cross connects continues to grow. In Section VI, we will present some experimental results using a two-state tip/tilt mirror, and investigate the output coupling loss issue. Finally, in Section VII, we will discuss some of the pros and cons of the White cell approach to this problem.

II. White Cell

Since our cross connect is based on the White cell, we will review its operation briefly. The White cell [8], [9] is familiar to spectroscopists, who have been using it for decades to cause a light beam to pass multiple times through a gaseous sample in order to measure the absorption of low-pressure gases. It consists of three spherical mirrors, as shown in Fig. 1(a). One mirror faces the other two, and is separated from them by a distance equal to their radii of curvature R, which is the same for all three mirrors. The center of curvature of the mirror M on the left is located directly between the mirrors A and B on the right. The centers of curvature of A and B (CCA and CCB) are located on Mirror M, separated from each other by a small amount 2δ. Below Mirror M in the figure is an input turning mirror.

The operation of the White cell is as follows. A beam enters the cell by being imaged to a spot on the input turning mirror [see Fig. 1(b)]. The turning mirror is tipped such that the light is directed to Mirror A. Since Mirror A is a distance $R = 2f$ from the input plane, where f is the focal length, mirror A reimages the input spot to a new spot on the same plane ($2f$–$2f$ imaging, with a magnification of -1). The new spot will be located an equal and opposite distance d_1 from A's center of curvature. We call this spot bounce 1.

Since Mirror M is also located a distance of $R = 2f$ away from Mirror A, it images the light in the plane of Mirror A to the same plane, again with minus one magnification, so that whatever the light distribution is on Mirror A, it reappears on the other side of M's center of curvature. That is, the light from A is reproduced at B. This is an important feature of the White cell. Since the light from A is imaged onto B, as long as these two mirrors are the same size, light can be imaged back and forth between them many times without additional diffraction losses from the edges of the mirrors and without walkoff. This is critical in spectroscopy since losses should be attributable to absorption, not diffraction. Furthermore, the beam divergence can be significant if the spots are small as would be the case in an optical cross connect.

Next, spot 1 acts as an object for Mirror B [see Fig. 1(c)] which produces a new image on Mirror M, called bounce 2. The new spot is an equal and opposite distance from CCB. Mirror M images the light from B back to A, and the process continues.

The odd-numbered spot progress upward and the even-numbered spots progress downward, as shown in Fig. 2(a). Here, we are looking at the front of Mirror M. We have indicated the locations of the centers of curvature CCA and CCB. Seventeen bounces are shown, and an output turning mirror has been added to extract the beam from the White cell after all of the bounces have been completed.

The number of bounces a beam makes is determined by the overall size of Mirror M, and the alignment of White cell mirrors A and B. We emphasize that the spot locations depend entirely on the alignment of the two Mirrors A and B. This will become important when we replace Mirror M with a MEMS mirror in Section III, and the spots are made to land on specific pixels.

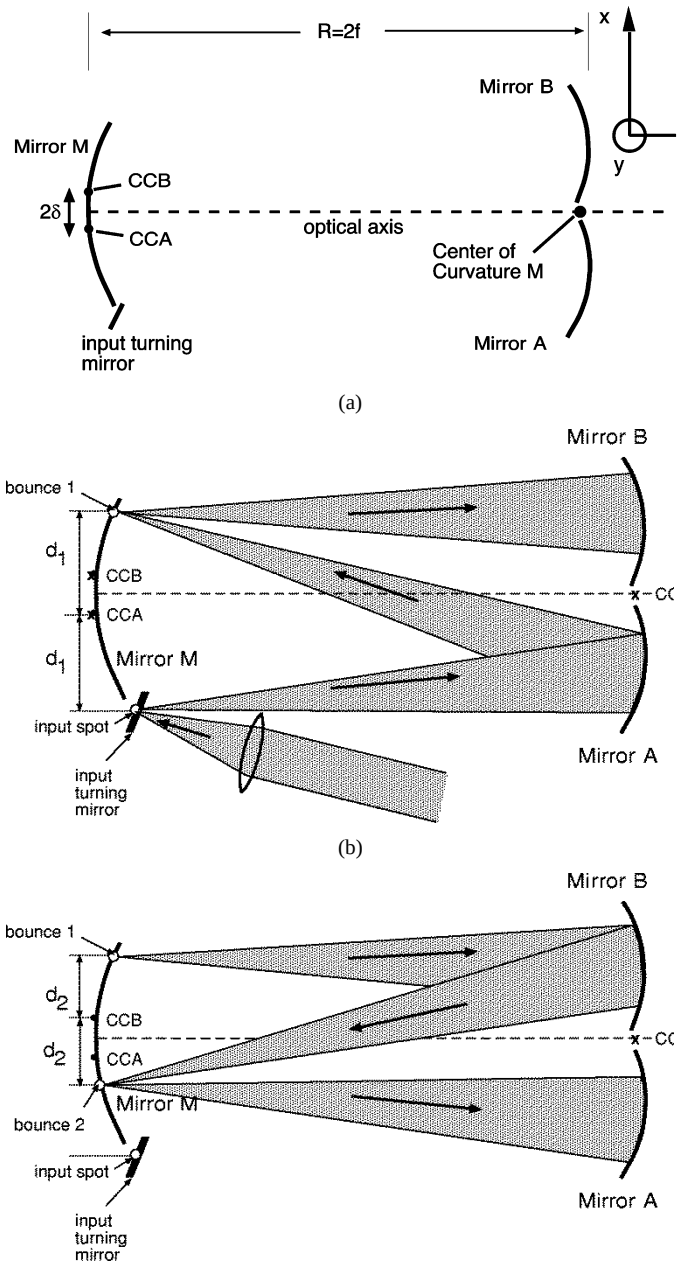

Fig. 1. (a) White cell consists of three identical mirrors, A, B, and M, separated by a distance equal to their radii of curvature. The centers of curvature (CCs) are located as indicated. (b) Mirror A images a spot on the input turning mirror to a new spot on Mirror M, an equal and opposite distance d_1 from A's center of curvature. (c) The image produced by A acts as an object for B, which produces a new image a distance d_2 from CCB. Mirror M also images light from one side of its optical axis to the other (magnification -1), meaning that light from A is imaged to B and vice versa. Thus, there is negligible diffraction losses from these mirrors.

Next, suppose we introduce some additional beams into the White cell, as shown in Fig. 2(b). We have used different shapes for each beam so their spot patterns can be distinguished. Each input spot results in a different spot pattern. In fact, the number of input spots can be very large (thousands). Each represents a different input signal. None of the bounces from any of the beams will strike any spot from another beam nor any spot already hit by the same beam. The spot patterns for each input beam are unique.

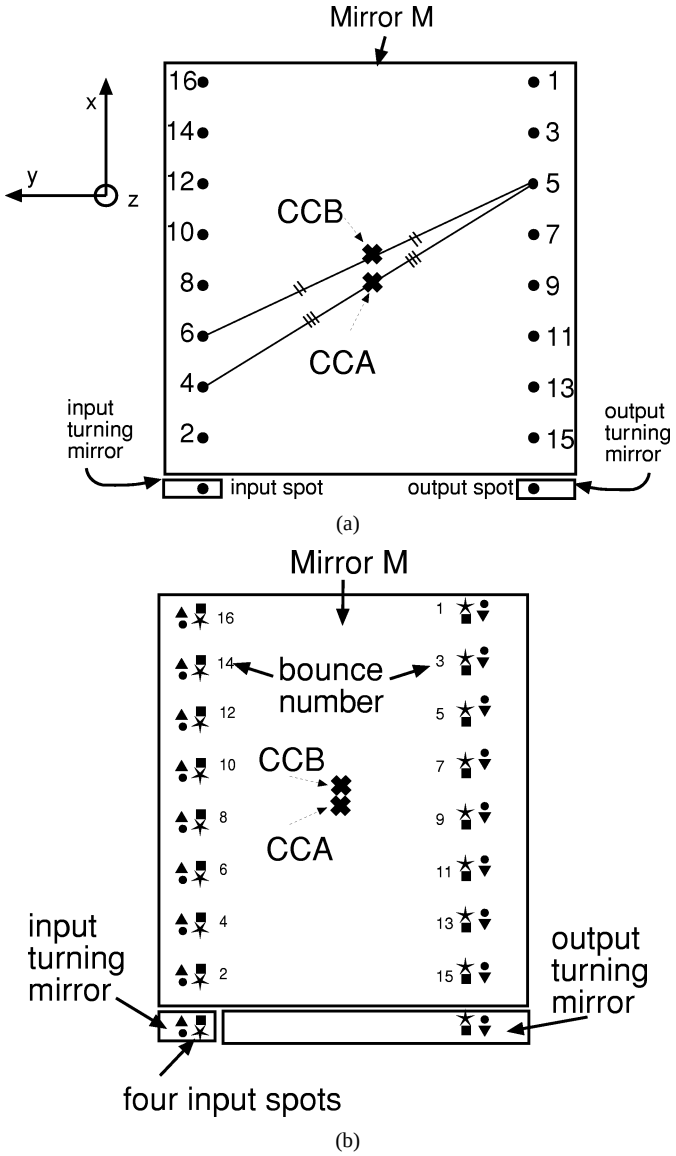

Fig. 2. Spot patterns in a simple White cell. (a) One input beam. (b) Four input beams. So far all beams emerge at the right hand side of the output turning mirror.

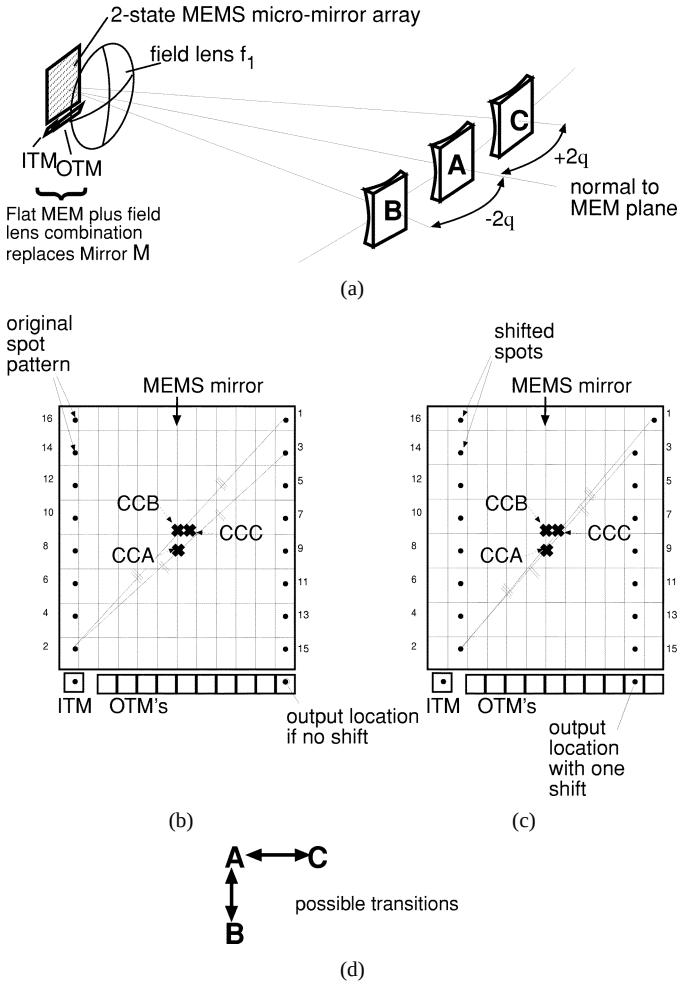

Fig. 3. White cell can be adapted to create a linear optical interconnection device by replacing Mirror M with a MEMS mirror and a lens. (a) If the MEMS mirror has two micromirror tip angles $\pm\theta$, then one can construct two White cells. Mirrors A, B, and the MEMS mirror/lens combination form one White cell and A, C, and the MEMS mirror/lens combination form the other. Light can be switched from one White cell to the other by appropriately tipping the micromirrors. (b) The spot pattern for a single beam all of whose pixels are tipped to $-\theta$ traces out this spot pattern and emerges at output region 0. The spot pattern for only a single input beam is shown to simplify the diagram. (c) If Mirror C's center of curvature (labeled "CCC") is located in a different position than B's, then the spot pattern is altered when a beam is sent to C. If the beam is sent to Mirror C one time, after the first bounce, and remains in the AB cell thereafter, the spot pattern indicated results. The beam exits the cell in a new location. (d) The connectivity diagram for this device.

Thus far, we have described only a White cell, and not a switch. We have established the spot patterns and shown that multiple beams can circulate simultaneously. So far, all of the beams emerge from the White cell at the lower right corner. We now have to cause those spot patterns to vary so that one may control the output locations of each spot. In the next section, we will do this by replacing Mirror M with a spatial light modulator. We will allow each spot from each beam to strike a different pixel. One will then be able to switch the beams to White cells with different mirror alignment, thus altering the spot patterns and, therefore, the exit point.

III. Adapting the White Cell to Optical Interconnection

In the White cell, the location at which a spot leaves the cell is determined entirely by the locations of the centers of curvature of the White cell mirrors, Mirrors A and B. In this section we will modify the White cell so that we can control the output location. We will do this not by moving Mirrors A and B, but rather by adding one additional spherical mirror, Mirror C, whose alignment is slightly different.

We begin by introducing a spatial light modulator, specifically an MEMS micromirror array. We will take the MEMS mirror to be a tip/tilt micromirror array (as opposed to a piston/ membrane style MEMS mirror). Suppose each micromirror can tilt to either one of two different positions, $\pm\theta$. An example of such a MEMS mirror would be the Texas Instruments Digital Micromirror Device (DMD), used in computer projection systems. This MEMS mirror will replace Mirror M. Since the MEMS mirror array is assumed to be planar, we must also add a field lens f_1, placed in front of the MEMS mirror as shown in Fig. 3(a), to replace the imaging function of Mirror M. The input turning mirror (ITM) and output turning mirror (OTM) are also behind the lens.

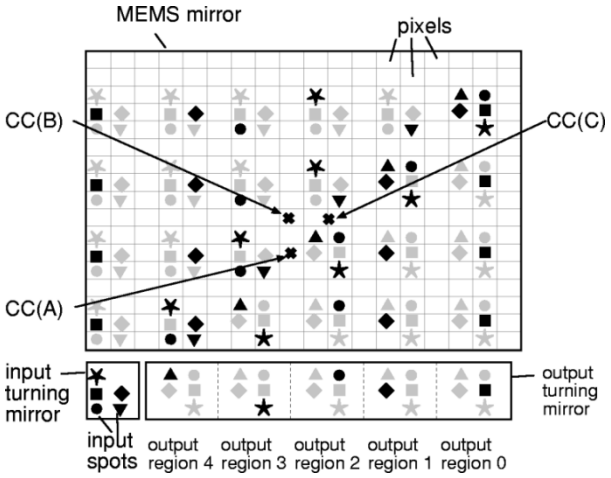

(e)

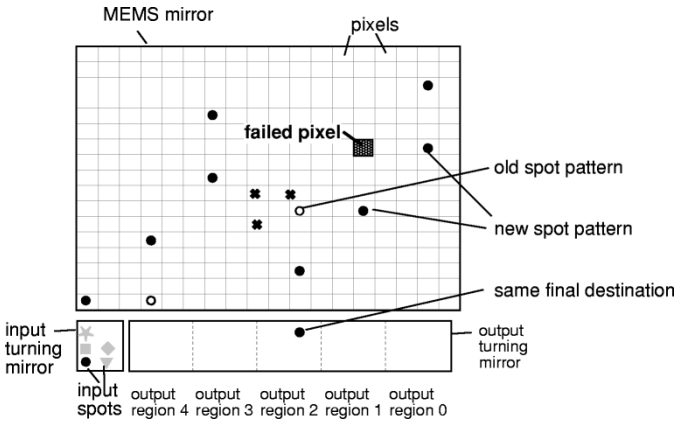

(f)

Fig. 3. *(Continued.)* White cell can be adapted to create a linear optical interconnection device by replacing Mirror M with a MEMS mirror and a lens. (e) Spot patterns for a 5×5 cross connect. Five input beams, each represented by a different shape, enter via the input turning mirror. The gray shapes indicate the possible spot patterns, and the black shapes show the chosen patterns for a particular connection. Here the "square" beam is sent to output 0, the "diamond" beam is sent to output 1, and so forth. (f) When a pixel fails, the beam may be routed in a variety of different paths. The pixel needed by the "circle" beam on the third bounce is broken, so it waits until the next bounce to go to Mirror C and obtain its shift.

In the figure, we see three spherical mirrors where before there were two. Mirror A is aligned on the normal to the MEMS mirror plane. Mirror B is on an axis at -2θ and Mirror C is on an axis at twice the tip angle $+2\theta$.

Consider some particular input spot in the array of spots on the input turning mirror of Fig. 2(b), reproduced in Fig. 3(b). Let us suppose that each micromirror that this beam will strike is tipped in the same direction $-\theta$. The beam goes from the input turning mirror to Mirror A, which creates the first bounce back on the MEMS mirror. Since the pixel is tipped to $-\theta$, the beam will be reflected at an angle perpendicular to the MEMS mirror plane and be sent to Mirror A. That is, Mirrors A and B form a White cell with the MEMS mirror and lens f_1. Light bouncing back and forth in this White cell will trace out the prescribed spot pattern for this beam, and emerge at the far end of the output turning mirror, just as in Fig. 2. Similarly, all other spots would emerge on the output turning mirror, an image of the array of input spots.

What if one pixel is tipped to $+\theta$? Then light for that particular beam, if it is coming from A, would be reflected at $+2\theta$, and be sent to C. Let us assume this happens after the first bounce on the MEMS mirror. Fig. 3(c) shows the spot pattern for this beam. Since the light now goes to Mirror C, the next image appears at an equal and opposite distance from C's center of curvature CCC. We choose to locate CCC such that the next spot forms in the same row, but is moved over by one column. This is indicated in the figure. The next pixel is also tipped to $+\theta$, and the light returns to A. Thus, A and C also form a White cell. The location of subsequent spots is determined by the subsequent pixel tilts, which control whether light goes to the AB White cell or the AC White cell on each bounce.

If the rest of the pixels that the light beam encounters are all tipped to $-\theta$ such that the light thereafter remains in the AB White cell, then the spot emerges on the output turning mirror one column over from its original output location. Similarly, if the light is sent to Mirror C two times, then the output spot will emerge two columns over, and so forth.

The connectivity diagram in Fig. 3(d) shows the possible transitions among the spherical mirrors. Since we have stipulated only $\pm\theta$ as allowed micromirror positions, there is no pixel tip angle that will send light directly from C to B. The light must be returned to Mirror A on every alternate bounce.

A. Number of Ports

Next, let us discuss the numbers of inputs and outputs. The number of inputs is determined by the number of spots on the input turning mirror, and is arbitrary. Recall that *each* of these spots traces out a unique spot pattern, and thus, strikes a unique set of pixels. Each of the inputs can be delivered independently to any of the possible outputs, which are defined as separate output turning mirrors.

The number of possible outputs is determined by the total number of possible shifts for a given number of bounces. In this case, a shift is made every time the light goes to Mirror C, but this can only happen after odd-numbered bounces. Thus, the number of possible outputs N is given by the number of possible shifts, plus one for the case of no shift

$$N_{\text{linear}} = \frac{m}{2} + 1 \tag{1}$$

where m is the number of bounces. We call this a "linear" optical interconnection device since the number of outputs is proportional to the number of bounces. For example, suppose $m = 8$. A given input spot can be directed to any of five different output locations. Fig. 3(e) shows five input spots. Each beam is represented by a different shape. The black shapes indicate the spot patterns for each input. Each input in this example is sent to a different output; for example, the circle is directed to output 2 while the triangle exits the White cell at output four. The gray symbols indicate all of the *possible* pixels each beam might strike.

Typically, the number of inputs would be equal to the number of outputs, but that is not required. To implement a 1024×1024 cross connect, then, would require a prohibitive 2046 bounces. Clearly, a more efficient technique is needed, and we will present some much more powerful designs in Section V. Before moving on, however, we wish to establish some points about the White cell.

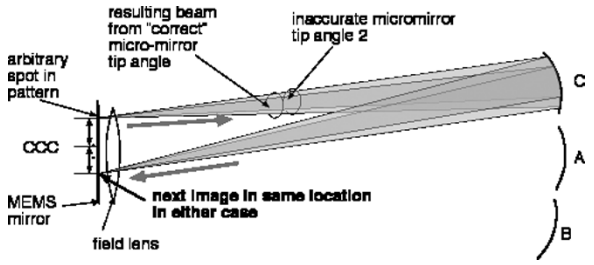

Fig. 4. Micromirror tip angle does not have to be carefully controlled. If the pixel tip is a little off, the beam strikes the spherical mirror in a slightly offset position, but the next spot still appears in the same place.

B. Redundancy

There is built-in redundancy. Consider the progression of the "circle" beam of Fig. 3(e), repeated in Fig. 3(f). Suppose the indicated pixel fails. There are two other ways to get to output region two, one of which is shown in solid circles. The open circles represent the previous spot pattern (before the failure).

This built-in redundancy is unique among optical switches. When a pixel fails in other optical interconnections, at least one connection is no longer possible, for example in the N^2 type. In the 3-D $2N$ designs, one input or output (or both) is out of commission until the MEMS chip is replaced.

The number of alternate paths depends on the output selected. In the examples of Fig. 3, the first and last output have no redundancy at all, since there is only one way to get to them. This can be remedied by adding an extra bounce so that there is always at least one alternate path.

C. Robustness

The system is robust in another way. In other optical switches, the micromirrors must be aimed very precisely because they steer the beams to the outputs. In the White cell, the steering is done only by the fixed spherical mirrors. They can be aligned precisely and left alone. The MEMS mirrors serve only to select which spherical mirror is visited.

D. Micromirror Tip Angle Accuracy

In fact, the tip angles of the micromirrors does not have to be particularly well controlled. Fig. 4 illustrates this point. Here, the beam coming from an arbitrary pixel is on its way to Mirror C. The next image is formed at an equal and opposite distance from CCC. The beam path for the "correct" MEMS tilt angle is shown to hit Mirror C and image properly. If, however, the pixel has some tip error, the beam strikes Mirror C in a different location, but the next spot still appears in exactly the same place. The spherical mirror is made slightly larger to accommodate the possible offset. The MEMS accuracy required, therefore, depends only on how large one is willing to make the spherical mirrors. We currently design for a tip accuracy of $\pm 1^\circ$, which is far easier to achieve with a MEMS mirror than the tiny fractions of degrees required in other devices.

E. Output Regions

Each input spot can be directed to any specific output region, but within that region the arriving beam may appear anywhere, and the beams may arrive from different angles depending on which White cell was visited last. Therefore, we need a way to combine the beams—to superpose them on one spot and make their arrival angles all of the same. We will present a solution in Section IV.

F. Loss

The loss consists of the loss inside the White cell and the output coupling loss, for example going into fiber. The loss inside the White cell depends on the mirror reflectivities, the MEMS mirror loss, and the number of bounces. It is crucial to reduce the number of bounces and still support a very large cross connect. We will discuss this loss further in Section V. The other loss is incurred when coupling the output beams into a single-mode fiber and, in Section VI, we present some experimental results.

IV. Combining the Beams at the Outputs

We noted earlier that any input directed to a particular output will land in a different place within that output region. Once a given input has reached the correct output region, the spots must all be made to land in the *same* spot, for example, on a detector or a fiber core. This is nontrivial in the White cell because in addition to arriving at different locations, the beams may arrive from different angles, a factor that will seriously affect coupling into a fiber. There are actually two issues of concern here. The first has to do with which White cell a beam is arriving from when it reaches the output region. The other arises from the particular output location within that region that the spot.

Fortunately, the most severe of these is also the easiest to fix. Consider the linear cell of Fig. 5(a). In this case, we have set m to an odd number of bounces. The "circle" beam is directed to output 1, and is shifted at the first opportunity, so that its final bounce come from mirror B. The "square" beam, on the other hand, could not be shifted on the first bounce due to a failed pixel. It was rerouted so that it was shifted on the last bounce, thus arriving at the output from Mirror C. Whatever is used to combine the beams must allow for these different angles. One simple way to solve this problem is to add one additional bounce. Then, regardless of the output selected, all beams can be sent to Mirror B on their last bounce.

The beams are all arriving from the same spherical mirror now, but each beam will arrive at any of several different locations within a specific output region, and their arrival angles will vary slightly, as shown in Fig. 5(b). These spots must all be superimposed, and for efficient coupling into an output fiber, they must also have the same angle.

Our solution is called the "trap door" beam combiner. We use a second White cell to march the spots across a field mirror, and each one falls through a trap door (a hole in the mirror, for example), and goes to the output. Each beam arrives at the same place and is coming from the same direction.

For our design of a beam combiner, we refer the reader to the White cell and its spot pattern described in Fig. 3(a). We will place a passive (nonswitching) White cell group behind the switch, which has as its input plane the output of the switch.

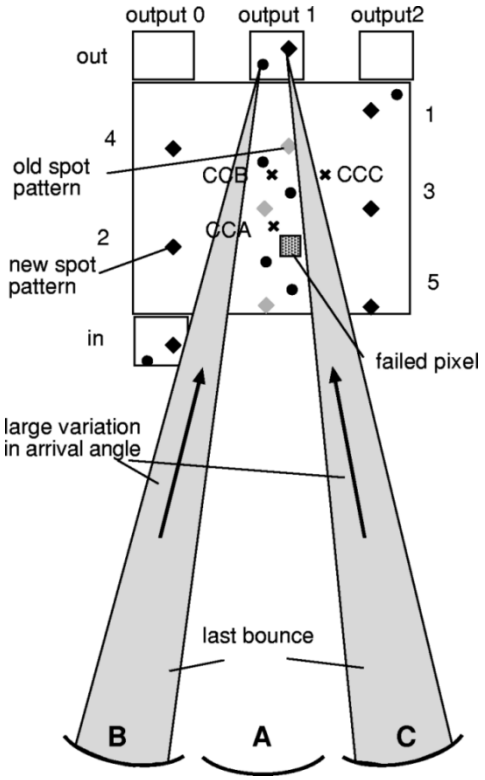

(a)

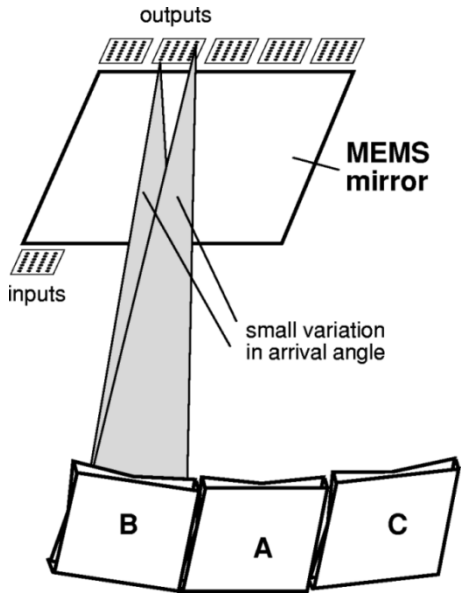

(b)

Fig. 5. Issues in combining the beams within an output region. (a) The beams may be arriving from different White cells. (b) Beams arriving at different points in the same output region will have different angles.

This is shown in Fig. 6. In the figure, the switch is on the right, and the beams are reaching the output areas as shown. They can pass right through, and be incident on the first of three spherical mirrors. There are three spherical mirrors, labeled A′, B′, and C′. These form White cells with an analog to Mirror M, call it M′, which in the drawing would be on the back side of the MEMS. The field lenses are not shown. The optics can be adjusted to place this analog mirror M′ in any convenient spot.

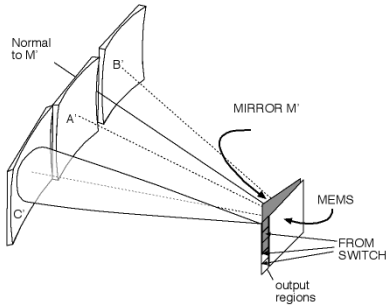

Fig. 6. Beam combiner is a White cell group located behind the output plane of the switch.

The plane M′ consists of a passive flat mirror that has fixed tilted micromirrors in some locations. These are essentially small prisms whose hypotenuses are coated with a high reflectivity coating, and they direct light at a particular pixel in a specific direction. This is in contrast to the switch itself, which has movable mirrors at every location that can tip to a variety of directions. In the beam combiner, the angles of the "pixels" are fixed. Also, somewhere in the plane of Mirror M′ is a series of holes through which the beams will eventually pass.

Let us assume, to begin with, that the output regions of the switch [Fig. 3(e)] each contains a linear array of spots (we will address a 2-D array of spots shortly). Fig. 7(a) shows the "input turning mirror," which is the input to the beam combiner and also the output of the switch. Actually, no physical mirror is needed (although field lenses, not shown, would be). Each row in Fig. 7(a) corresponds to a different intended output of the optical interconnect. In an optical interconnection device, most likely, only one position of the possible output spots in each array will actually be illuminated. Regardless of the position in the array at which the beam arrives, it should be directed to a single detector or optical fiber, corresponding to that row.

In the figure, we will consider two different outputs (of the switch). In the row containing the square, the fourth spot is lit, and in the row with the triangle the second spot is lit.

Now, let the light passing through the output region of the switch, which is the input to the beam combiner, be directed to mirror C′. This spot array is imaged by Mirror C′ to a new spot array in the upper right-hand corner of the figure. The region of the Mirror M′ where these spots land, and all of the spot locations in the same columns, consists of a series of fixed micromirrors all tipped to some angle θ. These tipped micromirrors send the beams to Mirror B′. The beams return to Mirror M′ in the lower left-hand corner, where there is another series of tipped micromirrors. At this point, the entire spot set has been stepped sideways by some distance greater than or equal to the spot array size. The tipped mirrors send the entire spot array back to Mirror C′ and forms another set of spots, at the top of the figure with dashed lines around each "pixel."

From here on in, the fixed micromirrors will be tipped such that the light circulates only between A′ and B′. This can be arranged to be flat, e.g., the plane of Mirror M′, so that no further micromirrors are needed.

We now set the distance δ' between the centers of curvature of mirrors A′ and B′ to be smaller than that between B′ and C′. We choose it such that the sideways step will be also smaller,

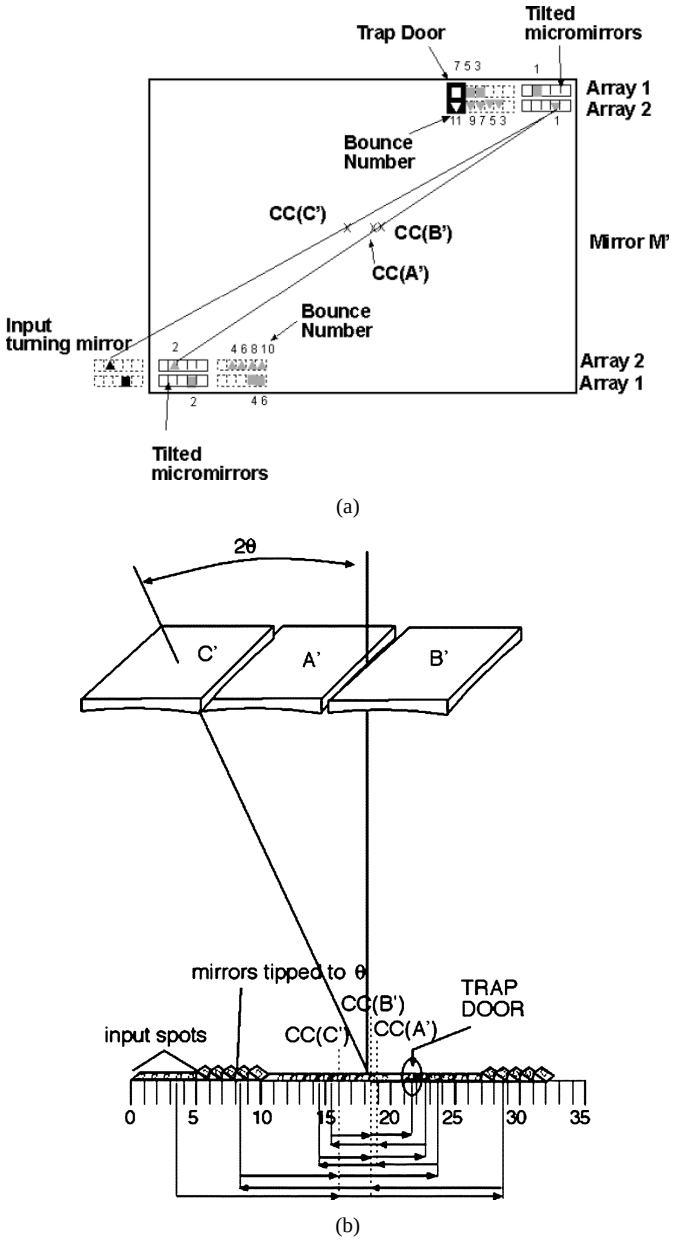

Fig. 7. (a) Spot pattern in the combiner. Each beam first strikes two sets of fixed tipped micromirrors, sending the light to Mirrors C′ and B′, and stepping the spot pattern over one array width. After that, the light circulates only between B′ and A′, and the spots shift over one pixel at a time until they fall through the trap door. (b) Perspective view for one particular row.

now equal to the spacing between two spots in the array. Some of the spots now land on pixels that have been previously visited by another spot, but the direction of tilt of the micromirror is the same, so there is no problem. As the beams continue to bounce, each will move one spot over on each bounce.

Fig. 7(a) shows the bounce numbers for each of our two cases. The square beam emerges from the White cell by falling through the trap door on bounce number 7, while the triangle beam falls through its trap door on bounce number 11.

Let us follow one beam carefully. Fig. 7(b) shows a 3-D picture and is laid out on a grid to show the spot patterns. Consider the fourth spot in the input array of Fig. 7(b). The light from this spot goes first to Mirror C′. This mirror's center of curvature is located 12 units from this input spot, so it is reimaged at location $4+2(12)=28$. There is a tipped mirror here, sending the light next to B′. The center of curvature of B′ is 10 units to the left, so the next image appears at location $28-2(10)=8$. The tipped mirror at this location sends the light back to C′, creating an image at location 23. Now, the mirrors are flat. Light goes from here to A′. Its center of curvature is halfway between locations 18 and 19, creating the next image at location 14. From now on, the light circulates only between B′ and A′. At the next bounce, the beam strikes pixel 22, which has already been visited on the last bounce by the fifth beam in the input array, but we do not care. Since their centers of curvature are spaced one-half unit apart, the spots now form one unit apart on each bounce.

By bouncing exclusively between mirror A′ and B′, any spot of a particular array will scan all of the positions ahead of it, eventually landing on each one. Suppose that we place a hole in the location labeled "trap door" in Fig. 7. The first spot in the array will fall through this hole on its third bounce, and go out to the output fiber or detector that will be paced behind it. The other spots, however, are still striking mirrors, and continue bouncing in the A′–B′ White cell. The second spot falls through the hole on the fifth bounce, the third spot on the seventh bounce, etc.

Note that the spots now all arrive at the same location, with the same angle of propagation. The tradeoff is that they arrive at different times. If variations in latency are a problem, the beams can be predelayed in advance (for example, in another White cell-based or other optical delay line [9]) such that when they go through the combiner they exit at the same time as well. The tradeoff is added complexity.

For a large switch with many inputs and outputs, the input spots are more likely to be in a 2-D array. In this case, a second White cell group can be added behind the first to combine the rows of each region to a single spot.

The loss of the beam combiner is expected to be very small, since all of the elements are passive, fixed, and can be treated with very high-reflectivity coatings.

V. Higher Order Polynomial-Based Optical Interconnections

So far, we have used a linear White cell-based optical interconnection device as a simple example to illustrate the operation principles. We kept the numbers of inputs and output small to simplify the figures. The goal, however, is to have a very large number of inputs and outputs, which, for the linear device, would require a prohibitive number of bounces. In this section, we discuss several designs that allow a large number of ports with fewer bounces, and thus, less loss. All of these exploit a big advantage of the White cell, which is that a very large number of beams can circulate simultaneously, each with a unique spot pattern. Very similar devices have been described for optical true-time delay [11] in which multiple White cells share a MEMS mirror device. In time delay applications, the White cell mirrors are aligned the same but the lengths of the White cells are different. There, the spot patterns must be the same regardless of the path selected. In interconnection devices, we want the lengths of the White cells to be the same, to maintain equal latency, but the spot pattern should differ, which is achieved by changing the alignment of the fixed spherical mirrors, as it was in the linear cell described above.

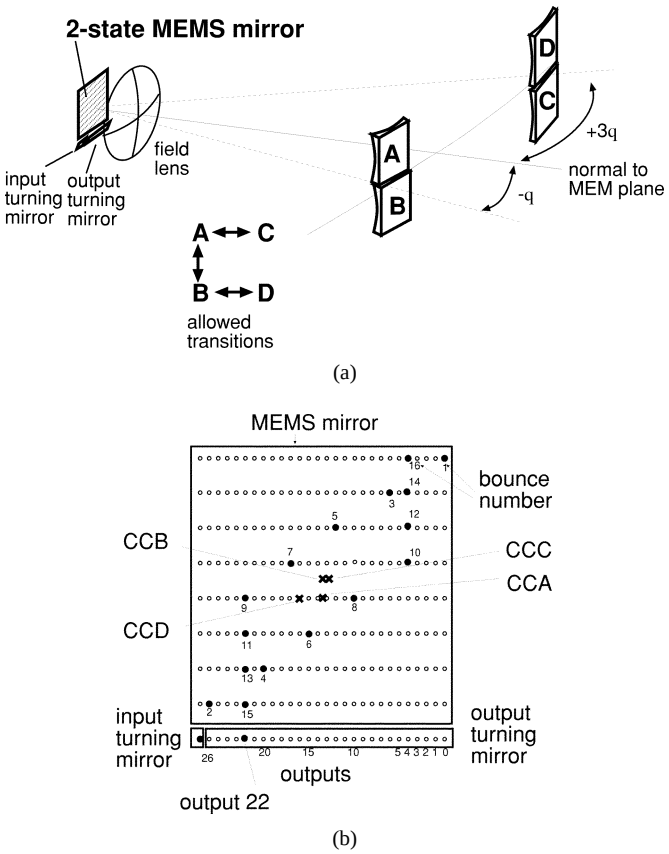

Fig. 8. (a) Quadratic cell uses a two-state MEMS mirror and four spherical mirrors. (b) The resulting spot pattern for a single input being directed to output number 22. Additional input spots are possible but not shown for simplicity.

A. Quadratic Interconnection Device

Let us assume the same two-state MEMS mirror as we used in the linear cell, but this time, we will arrange the spherical mirrors differently. In Fig. 8, we form the first White cell by placing Mirrors A and B one above the other along an axis at $-\theta$ (one of the allowed pixel normals). Light from A is reflected back to B and vice versa so long as the pixels are set to $-\theta$. A and B form a White cell.

If a pixel is turned to $+\theta$, then light coming from this micromirror will be reflected from the MEMS mirror at an angle of $+3\theta$ with respect to the normal to the MEMS mirror plane. We place two more mirrors there, C and D along the $+3\theta$ axis. Light coming from A will go to C and light coming from B will go to D. Thus, A and C form a second White cell, and B and D form a third.

Light must always travel from an upper mirror to a lower mirror. The connectivity diagram is also shown in Fig. 8(a). It is not possible from light to go directly from C to D; a pixel tip of $-\theta$ returns the light to the AB cell, and a pixel at $+\theta$ deflects the light at $+5\theta$, a direction not being used here.

Let us call AB the null cell. That is, light circulating exclusively in this cell will trace out its original spot pattern and exit the cell at the zeroth location (no shift).

We will align Mirror C such that it shifts the spot pattern by one column

$$C \Rightarrow 1. \tag{2}$$

The total number of shifts (outputs) obtainable from Mirror C is the same as the number of times the light can go there. Since C is a lower mirror, light can only be sent there after odd-numbered bounces on the MEMS mirror. Furthermore, from the connectivity diagram of Fig. 4, when light goes to C it must return to A. It therefore requires two bounces to use Mirror C. We allow the light to visit C a maximum of $m/4$ times (saving another $m/4$ bounces for mirror D), where again m is the number of bounces. We can, thus, produce up to $m/4$ column shifts using this mirror alone.

We then align Mirror D's center of curvature such that when light is sent to it, it returns to the MEMS mirror shifted over by one more column than this, or $(m/4)+1$ columns

$$D \Rightarrow \frac{m}{4} + 1. \tag{3}$$

Mirror D might be considered a coarse adjustment, and Mirror C a fine adjustment. We also allow visits Mirror D a maximum of $m/4$ times.

Let us suppose there are 16 bounces. To direct a particular input spot to the first output, we set all of the pixels to $-\theta$, and light circulates in the AB cell, emerging at the far right position on the output turning mirror. To send a beam to the second output, we flip one micromirror, on any odd-numbered bounce, and send the light to C one time. To send it to output two, we flip two pixels and send the light to C twice, and so on. We can complete up to up to four single-column shifts via Mirror C using a 16-bounce system. We align Mirror D in this case to shift the spot by one column more than this maximum of four, that is to say five columns. Fig. 8(b) shows the centers of curvature for these mirrors. The spot pattern generated in a 16-bounce system for a single input beam to go to output #22 is shown. This beam is switched to C twice (shift by one column each time) and makes four visits to D (each producing a shift of five columns), producing a total shift of 22 columns.

The maximum number of shifts (outputs) is obtained when C and D are each visited $m/4$ times, or

$$N_{\text{quadratic}} = \underbrace{\left(\frac{m}{4}\right)}_{\text{visits to D}}\underbrace{\left(\frac{m}{4}+1\right)}_{\text{shift of D}} + \underbrace{\left(\frac{m}{4}\right)}_{\text{visits to C}}\underbrace{(1)}_{\text{shift of C}} + \underbrace{1}_{\text{no shift case}}$$

$$= \left(\frac{m}{4}\right)^2 + 2\left(\frac{m}{4}\right) \tag{4}$$

where again we add "1" to the total for the case where no shift is created. This device is quadratic in $m/4$. For 16 bounces there can be 26 different outputs.

The quadratic cell is significantly more capable than the linear cell. Recall that the linear cell required 2046 bounces to connect 1024 outputs. This quadratic cell reduces that by a factor of 20, requiring only 124 bounces. This is still far too many bounces to be practical, however.

The primary issue will be loss. There will be a loss each time the beam strikes A, B, C, or D (which will happen 124 times total in the quadratic optical interconnection cell) and each time the beam strikes the MEMS mirror (another 124 times). Even with high-quality dielectric coatings on the mirrors ($R = 0.999$), and

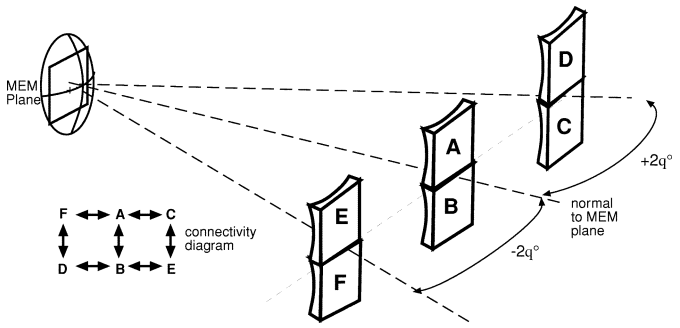

Fig. 9. "Quartic cell" using a three-state MEMS mirror.

good antireflections coatings on the field lens ($T = 0.995$), the losses from the spherical (fixed) mirrors alone would be 0.59 dB total. The MEMS mirror losses are harder to predict. Most micromirror MEMS of which we are aware use gold for the reflective coating, which at telecommunications wavelengths has an optimal reflectivity on the order of 0.98. This translates to an additional nearly 11 dB in 124 bounces, for a total of 16.8 dB. To bring this loss into a tolerable range (ideally <5 dB total) would require MEMS micromirrors with dielectric mirror coatings.

A secondary issue will be alignment tolerance. A misalignment in one of the spherical mirrors (A, B, C, or D) will be amplified by m, in this case 124. While such control can be achieved, we prefer to reduce instead the number of bounces.

We set as a goal to have twenty or fewer bounces, corresponding to a reflectivity loss of less than 3 dB total even with a gold MEMS. In the next section, we present some higher-order designs based on MEMs having more than two states.

B. Quartic Interconnection Device

Let us consider what might be achieved using a tip/tilt micromirror array in which each pixel has three stable states, instead of only two, and let us take these states to be 0° (flat), $+\theta$, and $-\theta$. Such a device has been reported in [12]. Fig. 9 shows how we might assemble several White cells. We place our null cell (A and B) on the axis normal to the MEMS mirror plane. When the pixels are flat, light goes back and forth between A and B, creating an unshifted spot pattern. If a pixel is tipped to $+\theta$, light reflects off the MEMS mirror at an angle of 2θ, and we place two more spherical mirrors (C and D) here. Similarly, we place two mirrors (E and F) along the -2θ axis.

Fig. 9 also shows the allowed transitions. In this case, light from D can go to B (pixel at $+\theta$), or to Mirror F (pixel flat). Similarly, light can go from C to E. Again, light always travels from an upper mirror to a lower mirror and vice versa. It is not possible for light to go directly from C to D nor from E to F. We observe that there are two loops in the connectivity diagram and that each loop is closed.

Let us assign half of our bounces to take place in the ACEB loop, and the other half in the ADFB loop. Considering the ACEB loop first, we can visit either upper mirror on every other bounce, which we allow up to $m/4\times$. Thus, we assign the shift of Mirror C to be one column, and the shift produced by Mirror E to be $(m/4 + 1)$ columns, as in the quadratic cell of Section V-A. Since each of these can be visited up to $m/4\times$, the maximum possible shift that can be obtained in $m/4$ bounces using just these two mirrors is the same as (4). Thus, we align Mirror F to produce a shift of one more than this or

$$F \Rightarrow \left[\left(\frac{m}{4}\right)^2 + 2\left(\frac{m}{4}\right) + 1\right]. \tag{5}$$

This shift can be implemented up to $m/4$ times also, producing a maximum shift using just A, B, C, E, and F of

$$\begin{aligned} N_{\mathrm{A,B,C,E,F}} &= \left(\frac{m}{4}\right)\left[\left(\frac{m}{4}\right)^2 + 2\left(\frac{m}{4}\right) + 1\right] + \left[\left(\frac{m}{4}\right)^2 + 2\left(\frac{m}{4}\right)\right] \\ &= \left[\left(\frac{m}{4}\right)^3 + 3\left(\frac{m}{4}\right)^2 + 3\left(\frac{m}{4}\right)\right]. \end{aligned}$$

The final spherical mirror produces a shift of one column more than this or

$$F \Rightarrow \left[\left(\frac{m}{4}\right)^3 + 3\left(\frac{m}{4}\right)^2 + 3\left(\frac{m}{4}\right) + 1\right]. \tag{6}$$

The total number of shifts (possible outputs) is obtained by visiting each mirror $m/4$ times, with one exception. We must use at least one bounce to go through the null cell, to get from one loop to the other. This means we can visit one mirror one time fewer. We choose to visit Mirror C less often to allow the transition. Since C produces a shift of one, the total number of possible outputs that can be accessed in m bounces is

$$\begin{aligned} N_{\mathrm{quartic}} &= \left(\frac{m}{4}\right)\left[\left(\frac{m}{4}\right)^3 + 3\left(\frac{m}{4}\right)^2 + 3\left(\frac{m}{4}\right) + 1\right] \\ &\quad + \left[\left(\frac{m}{4}\right)^3 + 3\left(\frac{m}{4}\right)^2 + 3\left(\frac{m}{4}\right)\right] \\ &= \left(\frac{m}{4}\right)^4 + 4\left(\frac{m}{4}\right)^3 + 6\left(\frac{m}{4}\right)^2 + 4\left(\frac{m}{4}\right) - 1 \\ &= \left[\left(\frac{m}{4}\right) + 1\right]^4 - 2. \end{aligned} \tag{7}$$

This number is quartic in $m/4$. Twenty bounces will address 1294 outputs. We have achieved our goal of obtaining 1024 output in 20 bounces or less. In [11], the specific mirror progressions for some key output conditions are given, and will not be repeated here.

Although the current record for optical interconnections is 1024×1024, we would like to have greater scalability and go to even larger cross connects, with comparable or fewer bounces.

C. Octic Interconnection Device

Now, let us postulate a MEMS mirror whose micromirrors have three stable states, as in the quartic cell, but let us allow some of them to tilt around a north–south axis and others around an east–west axis. This can be achieved with the same MEMS technology, with just a mask change. This will allow the construction of an interconnection device that can address a number of outputs that is proportional to the number of bounces raised to the power of eight. Let us suppose the mirrors have a stable flat position, and can additionally tip to θ ° in either the east and west or north and south directions.

Fig. 10 shows how we can add a pair of White cell mirrors in each of the 2θ directions, plus a pair directly in front of the MEM. The connectivity diagram is also shown. We can view this arrangement as two quartic cells, one in the east–west plane and the other in the north–south plane. We will allow one extra

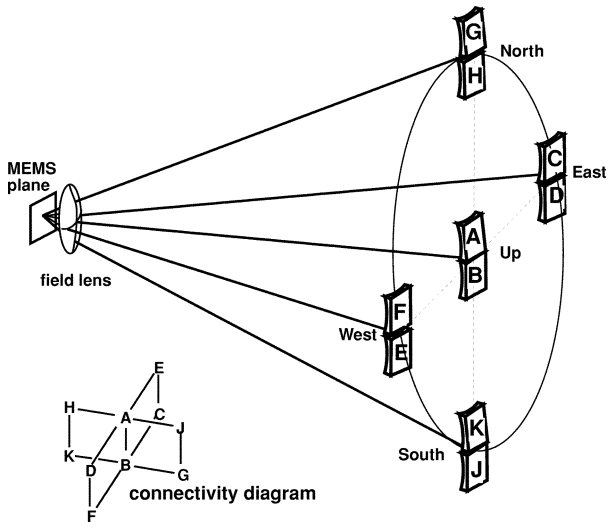

Fig. 10. "Octic" interconnection device using a three-state MEMS, some of whose mirrors tip east and west and others tip north and south. It is essentially two quartic cells combined, but can shift an input to any of 6399 outputs in 17 bounces.

bounce to transfer between these two quartic cells. Of the remaining $m-1$ bounces, we will set half to bouncing in the east–west quartic cell, and the other half to bouncing in the north–south cell. Thus, the fundamental counting increment in the octic cell will be $(m-1)/8$.

The mirrors will be aligned to shift the spot pattern by a number of columns as follows. In the east–west quartic cell, the assignments are similar to as before [compare to (2), (3), (5), and (6)]

$$\begin{aligned}
&\mathrm{C} \Rightarrow 1\\
&\mathrm{E} \Rightarrow \left(\frac{m-1}{8}+1\right)\\
&\mathrm{D} \Rightarrow \left[\left(\frac{m-1}{8}\right)^2+2\left(\frac{m-1}{8}\right)+1\right]\\
&\quad=\left[\left(\frac{m-1}{8}\right)+1\right]^2\\
&\mathrm{F} \Rightarrow \left[\left(\frac{m-1}{8}\right)^3+3\left(\frac{m-1}{8}\right)^2+3\left(\frac{m-1}{8}\right)^1+1\right]\\
&\quad=\left[\left(\frac{m-1}{8}\right)+1\right]^3. \qquad (8)
\end{aligned}$$

The maximum number of shifts that can be produced using just half the $m-1$ bounces and just the east–west quartic cell is given by

$$\begin{aligned}
N_{E-W} &= \left[\left(\frac{m-1}{8}\right)^4+4\left(\frac{m-1}{8}\right)^3+6\left(\frac{m-1}{8}\right)^2\right.\\
&\qquad \left.+4\left(\frac{m-1}{8}\right)-1\right]\\
&= \left[\left(\frac{m-1}{8}\right)+1\right]^4-2 \qquad (9)
\end{aligned}$$

which is different from (7) only by the counting increment in the parentheses. Thus, the next White cell mirror, let us pick G which is in the north–south plane, should shift the spot pattern by one more than this or

$$\mathrm{G} \Rightarrow \left[\left(\frac{m-1}{8}\right)^4+4\left(\frac{m-1}{8}\right)^3+6\left(\frac{m-1}{8}\right)^2+4\left(\frac{m-1}{8}\right)\right]. \qquad (10)$$

With an additional $(m-1)/8$ visits to G, we can shift up to N_{CEDFG} columns where, using (10)

$$\begin{aligned}
N_{\mathrm{CEDFG}} &= \left(\frac{m-1}{8}\right)\left[\left(\frac{m-1}{8}\right)^4+4\left(\frac{m-1}{8}\right)^3+6\left(\frac{m-1}{8}\right)^2\right.\\
&\qquad \left.+4\left(\frac{m-1}{8}\right)\right]\\
&\quad + N_{E-W}\\
&= \left[\left(\frac{m-1}{8}\right)^5+5\left(\frac{m-1}{8}\right)^4+10\left(\frac{m-1}{8}\right)^3\right.\\
&\qquad \left.+10\left(\frac{m-1}{8}\right)^2+4\left(\frac{m-1}{8}\right)-1\right]. \qquad (11)
\end{aligned}$$

Thus, the next mirror J should provide a shift of one column more than this. The remaining assignments are

$$\begin{aligned}
\mathrm{J} &\Rightarrow \left[\left(\frac{m-1}{8}\right)^5+5\left(\frac{m-1}{8}\right)^4+10\left(\frac{m-1}{8}\right)^3\right.\\
&\qquad \left.+10\left(\frac{m-1}{8}\right)^2+4\left(\frac{m-1}{8}\right)\right]\\
\mathrm{H} &\Rightarrow \left[\begin{array}{l}\left(\frac{m-1}{8}\right)^6+6\left(\frac{m-1}{8}\right)^5+15\left(\frac{m-1}{8}\right)^4\\ +20\left(\frac{m-1}{8}\right)^3+14\left(\frac{m-1}{8}\right)^2+4\left(\frac{m-1}{8}\right)\end{array}\right]\\
\mathrm{K} &\Rightarrow \left[\begin{array}{r}\left(\frac{m-1}{8}\right)^7+7\left(\frac{m-1}{8}\right)^6+21\left(\frac{m-1}{8}\right)^5\\ +35\left(\frac{m-1}{8}\right)^4+34\left(\frac{m-1}{8}\right)^3\\ +18\left(\frac{m-1}{8}\right)^2+4\left(\frac{m-1}{8}\right)\end{array}\right]. \qquad (12)
\end{aligned}$$

The total number of outputs accessible in this design for m bounces is

$$\begin{aligned}
N_{\mathrm{octic}} &= \left[\begin{array}{r}\left(\frac{m-1}{8}\right)^8+8\left(\frac{m-1}{8}\right)^7+28\left(\frac{m-1}{8}\right)^6\\ +56\left(\frac{m-1}{8}\right)^5+68\left(\frac{m-1}{8}\right)^4+48\left(\frac{m-1}{8}\right)^3\\ +16\left(\frac{m-1}{8}\right)^2+0\left(\frac{m-1}{8}\right)-1\end{array}\right]. \qquad (13)
\end{aligned}$$

Using $m = 9$ bounces yields only 224 shifts, which are not enough outputs for a competitive cross connect. The next choice of m is 17; using 17 bounces accesses 6399 different outputs. Specific mirror progressions are given in [11].

We have considerably increased the capability of the interconnection device, from 1294 outputs in 20 bounces in the quartic cell to 6399 outputs using 17 bounces in the octic cell. The number of inputs is strictly independent of the number of outputs, but one would usually choose them to be the same. Thus, with a single three-state MEMS mirror one could build a 6399 $\times$ 6399 cross connect using a single MEM, a lens, and ten mirrors.

We will discuss the pros and cons of the various White cell-based interconnection devices further in Section VII. In the next section, we will discuss some preliminary experimental results. First, we show a proof-of-concept demonstration of a linear well with one input and four outputs. Then, we measure the output coupling loss and compare it to the losses expected for other 3-D switches.

VI. Experiment

A. Proof of Concept

To demonstrate the operating principles of the interconnection device, we built the linear cell of Fig. 3. Fig. 11 shows the experimental apparatus. The MEMS mirror is on the left, and the three spherical mirrors are on the right. Our apparatus was built from parts borrowed from another project, and thus, not all of the mirrors have the same radii of curvature. Two of these had $R = 400$ mm and the other had $R = 600$ mm and all were 2 in in diameter. In order to preserve the imaging conditions of a White cell, the mirrors were, therefore, at different distances from the MEMS mirror. The field lenses and distances were as shown in the figure. The different focal lengths of the mirrors also necessitated using three field lenses (one different from the other two) instead of just one. These differences introduced unnecessary variations in latency but were otherwise harmless. The mirrors had aluminum coatings.

The MEMS mirror, at the left side of the figure, was a two-state tip/tilt micromirror device made by Texas Instruments. The chip has an array of approximately 400 $\times$ 600 micromirrors, each 16 μm^2 on a 17-μm pitch. The micromirrors can tip to either $\pm 10^\circ$. These MEMS mirror chips are not sold individually; we took apart a computer projector. The MEMS mirror was placed such that the normal to the MEMS mirror plane was parallel to the table. The MEMS mirror edges were at 45° to the table plane because the micromirrors tip around a 45° axis in the plane perpendicular to the table and we wished to keep all of our light beams parallel to the table to simplify fixturing.

The light source was a 5-mW HeNe laser, shown in the upper right. It was directed into the apparatus through a focusing lens and a beamsplitter that will be discussed later. The spot size was about 350 μm, much larger than the individual MEMS mirror pixels. We, therefore, used subarrays of 50 $\times$ 50 mirrors as our "pixels." We used four of these pixels as input and output turning mirrors as follows. The input beam was brought in at an angle of $+40^\circ$ with respect to the normal of the MEMS mirror plane. The spot was incident on a subarray of 50 $\times$ 50 micromirrors all tipped to $+10^\circ$. This caused the light to be directed into the arm labeled "B" in the figure. When the light returned to the MEM, the next pixel was set to -10°, and light was directed to Mirror A. We then took the beam to be "in" the cell. On subsequent bounces, the beam could be switched between the null cell (A and B) and the shifting cell (A and C).

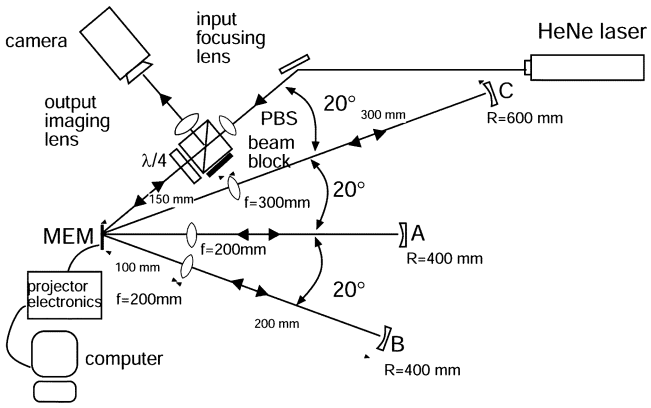

Fig. 11. Experimental apparatus for a proof-of-concept experimental demonstration of a 1 $\times$ 4 interconnection.

Two bounces were similarly used for output. After a visit to "A," the next pixel was set to -10°, sending the light to B, and the final pixel was set to $+10^\circ$, sending the light back out of the input path. A combination of polarizing beamsplitter and quarter wave $(\lambda/4)$ plate directed the output beam to a camera. The output position of a spot was then monitored on the camera as a function of the number of times the beam was sent to the shifting mirror C. We note that one could avoid the use of the polarizing optics by creating an output arm at -40°, but in this case one gets significant crosstalk from the Fresnel reflection of the input beam arriving from $+40^\circ$. The MEMS mirror has an uncoated cover glass.

Since we had only a single input beam, we did not construct the beam combiners described in Section IV.

When the light was directed only to the AB White cell, the output spot appeared at a location we will call output zero. When the pixels were addressed to send the light to Mirror C one time and B every other possible time, the output spot shifted over by a distance equal to twice the separation of the centers of curvature of Mirrors B and C. Each additional visit to Mirror C produced an additional shift of one "column," as expected. Thus, the operation of the device was verified.

The loss was not measured for the optical interconnection, but a nearly identical apparatus was used for another experiment, the key difference being the laser source. For the same optical components, including the MEMS mirror, but using a laser at $\lambda = 532$ nm, the loss was approximately 1.2 dB per bounce on the MEMS mirror (per round trip). The primary source of loss was determined to be due to diffraction from the MEMS mirror. This diffraction loss has two components, diffraction from the spaces between the micromirrors (1 μm wide), and diffraction from holes that appear in the center of each micromirror [13]. These tiny features caused diffraction angles of about 17° to the first zero, meaning considerable light was lost around the edges of the spherical mirrors, which were designed to capture a 20° cone only. This diffraction loss could be avoided by using a MEMS mirror with larger pixels.

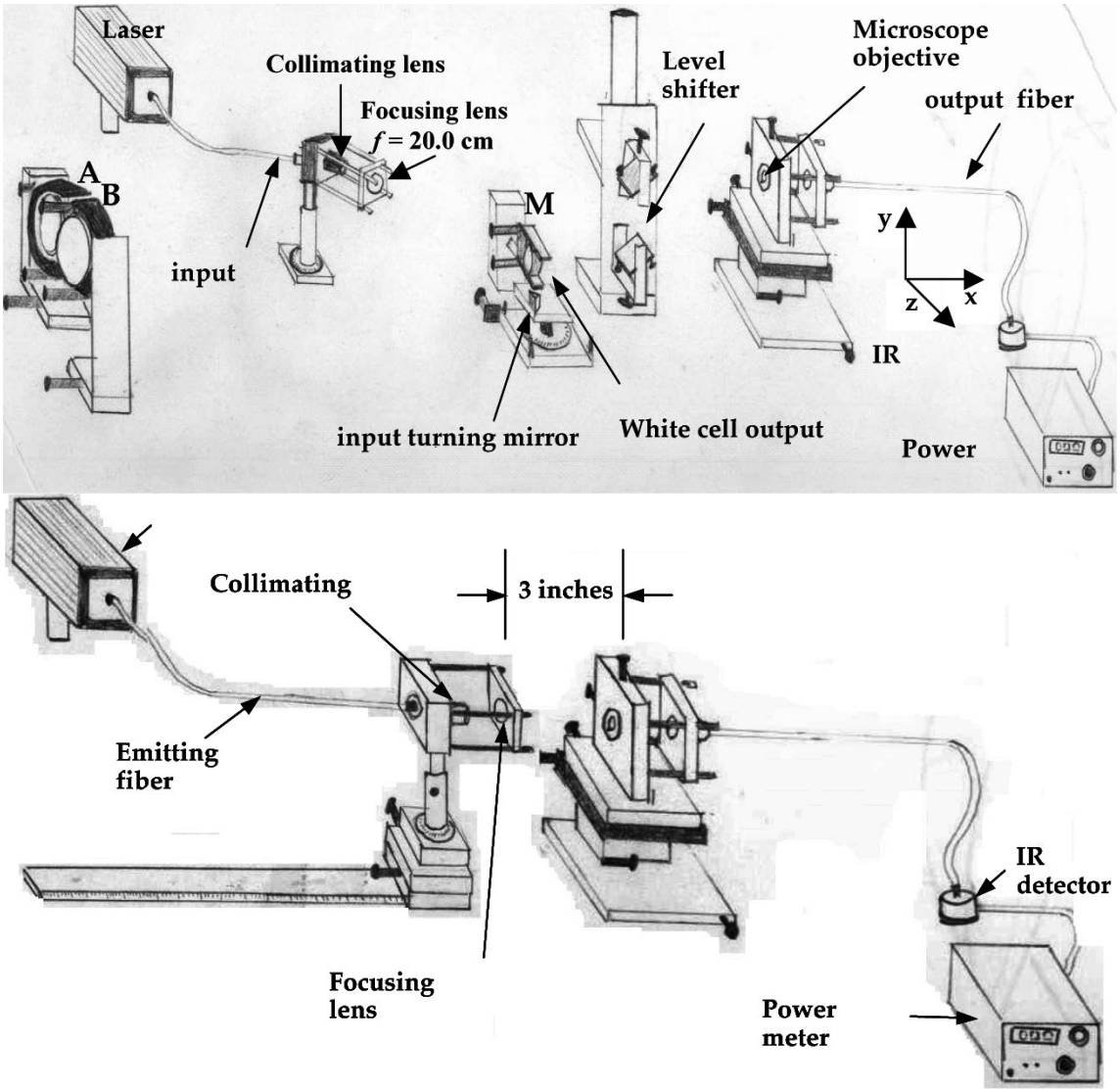

Fig. 12. Apparatus for comparing output coupling loss. (a) The White cell. (b) A fiber-collimated beam-fiber situation as is found in other interconnects.

B. Output Coupling

One source of concern was the question of whether coupling light from a White cell, in which the spots diverge rapidly, would be more difficult than coupling from a quasi-collimated beam as is done in other optical interconnection devices. To test this, we built a simple White cell using three dielectric spherical mirrors (no MEMS mirror). We also assembled an apparatus in which light from a fiber is collimated, propagates some distance, and is coupled into another fiber. We then compared the coupling efficiency.

The White cell apparatus is shown in Fig. 12(a). The source for this experiment was a single-mode fiber pigtailed 1.3-μm laser, and the fiber's output face was imaged onto the input turning mirror, which was gold. Two of the White cell mirrors (labeled A and B) are on the left in the figure. The field mirror, on which the spots form, is labeled M (as in "MEMS"). These all have a radius of curvature 0.5 m, and are coated with dielectric coatings of nominal reflectivity of 0.996.

The number of spots was controlled by adjusting the locations of the centers of curvature of A and B. As seen earlier in Fig. 2, the spots eventually walk off the field mirror. In the apparatus of Fig. 12, there is no output turning mirror, but rather, the beam passes the edge of the field mirror, coming to a focus in the plane of the mirror and diverging beyond it. The diverging beam passes through a level-shifter and is focused onto the output fiber, also single mode, using a microscope objective lens. This overall distance from the output of the White cell to the lens/fiber assembly was 16 cm. The output lens/fiber assembly had x, y, and z translational degrees of freedom, in addition to tilt around the y and z axes.

Each output coupling loss measurement was repeated four times using the following procedure. For each repetition, the output lens/fiber assembly was either disassembled and reassembled, or else all of the control knobs were turned in random directions by significant amounts. Then the lens and fiber were realigned from scratch, finding the optimal coupling efficiency.

For comparison, the fiber-to-fiber coupling apparatus is shown in Fig. 12(b). All components such as the laser, fibers, collimating lens, mounts, and output lens/fiber assembly were

the identical hardware as in Fig. 12(a). The light from the fiber was collimated, propagated a distance of three inches, and refocused into the output single-mode fiber. Again, each measurement was repeated four times and the output assembly was completely misaligned between measurements.

The output coupling loss in the White cell-to-fiber case was 1.91 $\pm$0.2 dB from the output spot to fiber output. For the fiber-to-fiber case, the result was 1.83 $\pm$ 0.2 dB. Thus, the output losses are the same to within the experimental error.

We also examined the losses in the White cell itself. The loss due to just the White cell was 0.028 $\pm$ 0.003 dB per round trip, well within the expected range for dielectric mirrors.

VII. Discussion

A. Loss

To be useful, an optical interconnection device must have low insertion loss. In our experiment, the greatest source of loss was the MEMS mirror itself. It must be remembered, however, that the particular MEMS mirror array we used was chosen solely for its availability, and this device was not designed for telecommunications but rather image projection. A MEMS mirror designed for a cross connect should have gold or dielectric mirrors, and ideally would have no holes in the mirrors. Holes are usually present, however, as a means to remove the release layer via etching (the acid has to reach the material under the mirrors, in the release layer, and the dissolved material needs a way to escape). The smaller the holes, the less the fill-factor loss but the greater the diffraction from the tiny features and, thus, the larger the diffraction loss.

Apart from the micromirrors, the losses from the other optical components are small, despite the multiple-pass nature of the White cell. The output coupling loss will probably ultimately be the limiting factor in producing a high-throughput interconnection device, resulting from coupling a free-space beam into a single-mode fiber. We showed experimentally that this loss will not be any worse for the White cell than for any of the other free-space approaches.

B. Alignment

The White cell is surprisingly stable and easy to align, which may be part of why it has been in use all of these years. The alignment of the spots on the MEMS mirror pixels is controlled by the tilt angles of the two fixed spherical mirrors (the locations of their centers of curvature). In aligning the apparatus, one adjusts the mirrors until the last bounce is on the correct pixel. If that spot is in the right place, all of them are in the right places. Any error in the tilt of these mirrors will be multiplied by the number of bounces, one of many arguments for reducing the number of bounces whenever possible. On the positive side, the alignment of these mirrors is fixed. Also, we will beat to death the point that the alignment of the spots onto the output fibers is not controlled at all by the MEMS mirror. The MEMS pixels only choose which spherical mirrors are visited, and the MEMS mirror-pointing angle does not need to be precisely controlled.

C. Redundancy and Pixel Count

Optical interconnections based on MEMs are generally classified as $2N$ or N^2, based on the number of switches required to interconnect N inputs to N outputs. The N^2 designs are typically planar. For example, a row of N inputs is along one edge of the switch array and the N outputs are along an adjacent edge. To connect input 3 to output 27, one engages the switch in row 3, column 27 to intercept the light beam and direct it to the appropriate output (for example [6]).

Interconnections that are $2N$, on the other hand, are typically 3-D, with the inputs and outputs arranged in an array above the MEMS mirror ([14] is a classic example). This general approach has a big advantage: fewer pixels are required (so the number of switches on a single chip can be larger), so 3-D approaches will scale up to very large N's. The down side is that the micromirrors must be very accurately positioned in order to couple ultimately into a single-mode fiber, and in general a feedback loop for each pixel is required.

The White cell approach described here is also 3-D and highly scalable, but it requires more pixels that either of the other approaches. For a linear cell, the number of pixels required is $[(m/2)+1]^2$ for m bounces, or approximately $[N+1]^2$ pixels for N inputs and N outputs. A quadratic cell, on the other hand, uses a pixel count that goes as N^3. The quartic and octic cells would use more pixels still. This means that the White cell approach as described here will ultimately require a large MEMS mirror with more pixels than the other approaches. The good news is that this introduces redundancy. We showed in Section III that there are multiple paths by which a given input can reach a given output. For example, if input x must be shifted three times to reach output y, it can happen on any three of the total bounces. Thus, if a pixel fails, there exist many other backup paths for x to reach y. In all other interconnection devices, to our knowledge, if a pixel fails that connection is no longer possible.

MEMS mirror technology, if it progresses anything like very large scale integration technology has, will eventually produce very large arrays with large numbers of pixels. In fact, Texas Instrument's DMDs are up over an impressive million mirrors now. Therefore, the cost associated with increasing the pixel count of the MEMS mirror will not be an issue.

D. Complexity of MEMS Mirror Device

We presented several designs for optical interconnections, based on two- and three-state MEMS. The MEMS required for the White cell approach are digital, meaning they have a limited number of fixed states, as opposed to analog, in which each micromirror is required to be able to tip to any arbitrary angle within some cone. Analog mirrors have a more complicated mechanical structure, and generally require some type of feedback to set and maintain the desired tip angle. With digital mirrors, mechanical stops can be built in and the mirrors driven against them. Since the White cell does not require tilt-angle accuracy greater than a degree or so, these stops do not need precise control. Alternatively, one may wish to avoid stops because of stiction, in which case the flexibility in tilt angle is also a bonus.

E. Summary

We have proposed and experimentally proven the concept of an optical interconnection device based on the White cell. This is a strictly nonblocking free-space device that uses a single MEMS tip/tilt micromirror array combined with several spherical mirrors. Many light beams can circulate in the White cell simultaneously, and each beam traces out a unique spot pattern. By superposing these spots on the micromirrors, light can be directed to any of several White cells on any bounce. Each White cell produces either no displacement in the spot pattern, or displaces a beam's spot pattern by some number of columns. Each visit to one of the displacement-producing spherical mirrors shifts the spot pattern by some predetermined amount. By combining visits to the various White cells, a given input beam can be directed to a given output.

We first presented a linear cell, which produced a number of shifts that were proportional to the number of bounces. It used a two-state MEMS mirror like the Texas Instrument's DMD. Then, we showed how to produce a quadratic cell, which allowed many more outputs to be accessed for a given number of bounces. If we expand our horizons to three-state MEMs, a quartic cell results, and combining two quartic cells produces an octic cell. The octic cell can shift a given input beam to any of 6399 different outputs with just 17 bounces.

There are downsides to the White cell approach, however. One is that the number of pixels required is much larger than for other optical cross connection devices. That same high pixel count also supplies automatic redundancy, however, so that if some of the pixels fail all of the connections can still be made. Furthermore, in the higher order cells like that quartic and octic devices, one need not actually make every micromirror of the (for example N^3) array, although the overall dimension of the array will still need to be the same. Another snag is that in the White cell, the MEMS mirror losses must be very small, because unlike other switches, each beam strikes the MEMS mirror multiple times. This means that MEMS mirror for a White cell-based interconnection will require, at a minimum, high-quality gold coatings or possibly even dielectric high-reflectivity coatings. Although such devices are not commercially available there should be no technological stumbling block.

One of the key advantages of the White cell approach is that it has massive parallelism. The octic cell, for example, requires a MEMS chip, 10 spherical mirrors, and 10 lenses, whether it is part of a 256×256 cross connect or a 6399×6399 cross connect. Thus, the amount of hardware for a truly large switch is not great. A second advantage of this approach is that alignment of the spots depends only on the (fixed) alignment of the spherical mirrors, and not on the micromirror tip angle accuracy. Thus, the White cell does not require a feedback and support circuitry, and alignment should be straightforward to maintain.

ACKNOWLEDGMENT

This work is a development from a similar approach used to produce optical true time delays for phase array radars, developed in collaboration with Prof. S. A. Collins, Jr., of The Ohio State University, Columbus. The apparatus of Fig. 11 was largely designed and constructed by A. Rader.

REFERENCES

[1] B. E. A. Saleh and M. C. Teich, *Fundamentals of Photonics*. New York: Wiley, 1991.

[2] D. K. Probst, L. G. Perrymore, B. C. Johnson, R. J. Blackwell, J. A. Priest, and C. L. Balestra, "Demonstration of an integrated, active 4×4 photonic crossbar," *IEEE Photon. Technol. Lett.*, vol. 4, pp. 1139–1140, Oct. 1992.

[3] M. Okuno, K. Kato, R. Nagase, A. Himeno, Y. Ohmore, and M. Kawachi, "Silica-based optical matrix switch integrating new switching units with large fabrication tolerance," *J. Lightwave Technol.*, vol. 17, pp. 771–780, May 1999.

[4] T. Goh, M. Yasu, K. Hattori, A. Himeno, M. Okuno, and Y. Ohmori, "Low-loss and high-extinction ratio silica-based strictly nonblocking 16×16 thermooptic matrix switch," *IEEE Photon. Technol. Lett.*, vol. 10, pp. 810–812, June 1998.

[5] C. Marxer and N. F. de Rooij, "Micro-optical-mechanical 2×2 switch for single-mode fibers based on plasma-etched silicon mirror and electroststic actuation," *J. Lightwave Technol.*, vol. 17, pp. 2–6, Jan. 1999.

[6] L. Y. Lin, E. L. Goldstein, and R. W. Tkach, "Free-space micromachines optical switches with submillisecond switching time for large-scale optical cross connects," *IEEE Photon. Technol. Lett.*, vol. 10, pp. 525–527, Apr. 1998.

[7] D. J. Bishop, C. R. Giles, and G. P. Austin, "The Lucent LambdaRouter: MEMS technology of the future here today," *IEEE Commun. Mag.*, pp. 75–79, Mar. 2002.

[8] J. White, "Long optical paths of large aperture," *J. Opt. Soc. Amer.*, vol. 32, no. 5, pp. 285–288, 1942.

[9] J. U. White, "Very long optical paths in air," *J. Opt. Soc. Amer.*, vol. 66, no. 5, pp. 411–416, 1976.

[10] A. Rader and B. L. Anderson, "Demonstration of a linear optical true-time delay device using a microelectromechanical mirror array," *Appl. Opt.*, vol. 42, no. 8, pp. 1409–1416, 2003, submitted for publication.

[11] B. L. Anderson and R. Mital, "Polynomial-based optical true-time delay devices using MEMs," *Appl. Opt.*, vol. 41, no. 26, pp. 5449–5461, 2002.

[12] O. B. Spahn, E. J. Garcia, V. Easch, G. Grossetete, F. Bitsie, S. Mani, and J. Jakubsczak, "Optical performance of pivoting micromirrors," in MOEMS and Miniaturized Systems II, San Francisco, CA, 2001.

[13] L. J. Hornbeck, "Digital light processing for high-brightness, high-resolution applications," in Proc. Electron. Imaging, San Jose, CA, 1997.

[14] D. Bishop, R. Giles, and C. Roxlo, "Micromirrors relieve communications bottlenecks," *Photon. Spectra*, pp. 167–169, Mar. 2000.

Betty Lise Anderson (S'75–M'79–SM'95) received the B.S. degree in electrical engineering from Syracuse University, Syracuse, NY, in 1978 and the M.S. and Ph.D. degrees in material science and electrical engineering from the University of Vermont, Burlington, in 1988 and 1990, respectively.

She spent nine years in the industry, including at Tektronix, Inc., Beaverton, OR, GTE Laboratories, Waltham, MA, and Draper Laboratories, Cambridge, MA. She is currently with the Department of Electrical Engineering, The Ohio State University, Columbus. Her current research interests include analog optical signal processing, devices for optical communication systems, coherence, and semiconductor devices.

Prof. Anderson is a member of the Optical Society of America and the Society for Photoinstrumentation Engineers.

Victor Argueta-Diaz received the B.S. degree in telecommunication engineering from the National Autonomous University of Mexico, Mexico City, Mexico, in 1999 and the M.S. degree in electrical engineering from The Ohio State University, Columbus, in 2002.

He spent two years in the industry, working on optochemical sensors and wireless communication. He is currently in the Department of Electrical Engineering, The Ohio State University. His current research interests include devices for optical communication systems, photonic crystals, and optical sensors.

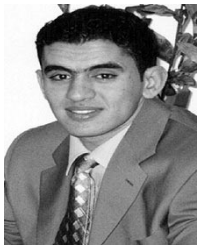

Feras Abou-Galala (S'00) received the B.S. degree in electrical engineering from the University of Qatar, Doha, Qatar, in 2000 and the M.S. degree in electrical engineering from The Ohio State University, Columbus, in 2003.

His current research interests at The Ohio State University include all-optical networking devices, QoS in optical communication networks, and optical signal processing.

Mr. Abou-Galala is a Member of the Society of Photo-Optical Instrumentation Engineers.

Gayathri Radhakrishnan received the bachelor's degree in electronics and communication engineering from Bharathiar University, Coimbatore, India, in 1998 and the master's degree in electrical engineering from The Ohio State University, Columbus, in 2000.

Until recently, she was with Corning Inc., Corning, NY, as a Senior Market Development Engineer for the Broadband and Premises markets. In this role, she was involved in new fiber development projects for this application space. She was also responsible for analyzing the different LAN and Fiber to the Home Network architectures and developing economic models for the same.

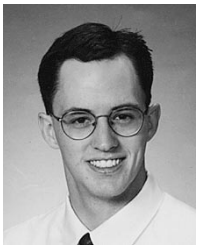

Richard Joseph Higgins (S'96–M'00) received the B.S. degree in electrical engineering from the University of Dayton, Dayton, OH, in 1998 and the M.S. degree in electrical engineering at The Ohio State University, Columbus, in 2000.

He was with the Battelle Memorial Institute, Columbus, OH, from 1995 to 2001. In 2001, he joined Optimer Photonics Inc., Columbus, OH, a recent Battelle spin off, as a Photonics Engineer, specializing in solid-state optical component integration.